Journal of Hydrology 653 (2025) 132767

Contents lists available at ScienceDirect

Journal of Hydrology

journal homepage: www.elsevier.com/locate/jhydrol

Research papers

Pressure management strategies for large-scale aquifer recharge: Mitigating the potential for injection-induced earthquakes

Ethan W. Conley [a,*], Cameron R. Chambers [a], John B. Ogunleye [a], Lars W. Koehn [a], Dan Holloway [b], Jamie Heisig-Mitchell [b], Martin Chapman [a], Mahesh Parija [a], Ryan M. Pollyea [a]

[a] Department of Geosciences, Virginia Tech, Derring Hall, Blacksburg 24061 VA, USA
[b] Technical Services Department, Hampton Roads Sanitation District, 1434 Air Rail Ave, Virginia Beach 23455 VA, USA

ARTICLE INFO

This manuscript was handled by Dongmei Han, Editor-in-Chief, with the assistance of Erin Marie King Haacker, Associate Editor

Keywords:
Induced seismicity
Managed aquifer recharge
Groundwater sustainability

ABSTRACT

Long-term groundwater withdrawals in coastal Virginia have led to declining groundwater levels, saltwater intrusion, and land subsidence, threatening regional water security and infrastructure. Managed aquifer recharge (MAR) through underground injection offers a promising solution to mitigate these effects. A large-scale MAR project is under construction in southeast Virginia to replenish the Potomac Aquifer, with a combined injection rate of up to ~ 189,000 m^3/day at two sites. The first site, scheduled for 2026, will begin operations with an initial injection rate of ~ 61,000 m^3/day. Given that the Potomac Aquifer lies unconformably above crystalline basement rock, injection-induced pressure transients may propagate into the basement, increasing the risk of injection-induced seismicity. To assess this risk, a regional-scale numerical model was employed, incorporating ensemble simulations with 50 models using spatially random and equally probable permeability distributions within the basement. The simulations of a 61,000 m^3/day injection scenario indicate significant pressure propagation into the basement, with fluid pressures reaching up to 40 kPa in some areas, which could be sufficient to induce seismicity. However, a ramp-up strategy for the injection rate, extending over a 12-month period, was found to effectively reduce the pressurization rate in the basement and mitigate the seismic risk. These results provide a probabilistic understanding of pressure changes in the basement rock and inform strategies for minimizing pressure transients that may induce seismicity while achieving effective aquifer recharge.

1. Introduction

With growing global populations, coastal groundwater resources face increasing stress (Casanova et al., 2016), driven largely by rising freshwater demand from expanding agricultural and industrial activities. This demand is leading to unprecedented levels of global groundwater scarcity (Gleeson et al., 2012). To mitigate groundwater scarcity, managed aquifer recharge (MAR) is emerging as an innovative solution for sustaining groundwater resources. In this context, MAR refers to a suite of engineered methods e.g., stream channel modification, bank filtration, and water spreading, that are designed to accelerate natural aquifer replenishment by surface water infiltration (Ringleb et al., 2016; Dillon et al., 2018; Zhang et al., 2020; Conley et al., 2022; Dillon et al., 2019). In addition, direct aquifer recharge via injection wells, also known as aquifer storage and recovery (ASR), has been implemented worldwide. Injection wells for ASR projects are reported between 50 and 900 m depth, and some ASR projects are now injecting partially treated surface water or purified water from municipal wastewater operations (Dillon et al., 2019). The global capacity of managed aquifer recharge (MAR) technology has grown significantly, rising from 1,000 million cubic meters per year (Mm^3/yr) in 1965 to over 7,500 Mm^3/yr by 2015 (Dillon et al., 2019).

Coastal Virginia has experienced significant groundwater depletion due to the overextraction of the Potomac Aquifer (Conley et al., 2022; Pollyea et al., 2022), the principle freshwater source in southeast Virginia. In confined aquifers, such as the Potomac Aquifer, overextraction not only diminishes groundwater resources, but also decreases fluid pressure and increases effective stress (Conley et al., 2022; Pollyea et al., 2022), causing land subsidence and saltwater intrusion. To mitigate these effects, the Hampton Roads Sanitation District (HRSD) is

* Corresponding author.
E-mail address: ewconley@vt.edu (E.W. Conley).

https://doi.org/10.1016/j.jhydrol.2025.132767
Received 10 August 2024; Received in revised form 6 December 2024; Accepted 17 January 2025
Available online 1 February 2025

developing a large-scale MAR project, called the Sustainable Water Initiative for Tomorrow (SWIFT), which is designed to replenish the Potomac Aquifer by injecting highly treated municipal wastewater at rates approaching 189,000 m^3/day (50 M gpd) (Conley et al., 2022; Pollyea et al., 2022). The SWIFT project comprises a network of injection wells located at two HRSD wastewater treatment plants. The first SWIFT site is currently under construction at the James River Wastewater Treatment Plant (JR WWTP) (Fig. 1), where aquifer recharge injections will begin in 2026 at a rate of 61,000 m^3/day (16 M gpd). The second SWIFT site is at the Nansemond Wastewater Treatment plant, which is planned to inject 129,000 m^3/day (34 M gpd) beginning in 2032.

Large-scale fluid injections into deep geologic formations are known to cause unintended seismic activity. This phenomenon is called injection-induced seismicity and became common throughout the central United States between 2009 and 2018 (Nrc, 2013) when re-injecting oilfield brine into deep geologic formations became a widespread practice in hydrocarbon recovery operations (Ellsworth, 2013; Weingarten et al., 2015; Ellsworth et al., 2015; Pollyea et al., 2019). Injection-induced earthquakes occur when increasing fluid pressure leads to a corresponding reduction in the effective normal stress exerted on a fault (Pollyea et al., 2013; Saar and Manga, 2003; Ge and Saar, 2022; Zoback and Hickman, 1982; Brown and Ge, 2018). As pressure transients propagate away from injection wells, earthquakes may occur when pore pressure intersects faults that are both critically stressed and optimally oriented with the regional stress field (Ge and Saar, 2022).

Currently, there is no linkage between underground MAR injections and induced seismicity; however, the SWIFT project is unique because the maximum recharge rate of up to 189,000 m^3 per day (50 M gpd) is comparable to the maximum rate of oilfield wastewater re-injection that occurred in Oklahoma in 2014, when there were over 550 magnitude-3 (M3) earthquakes, a substantial increase from the historical earthquake rate of ~ 1 per year (Pollyea et al., 2018). The geometry of the Potomac Aquifer further separates the SWIFT project from other aquifer recharge

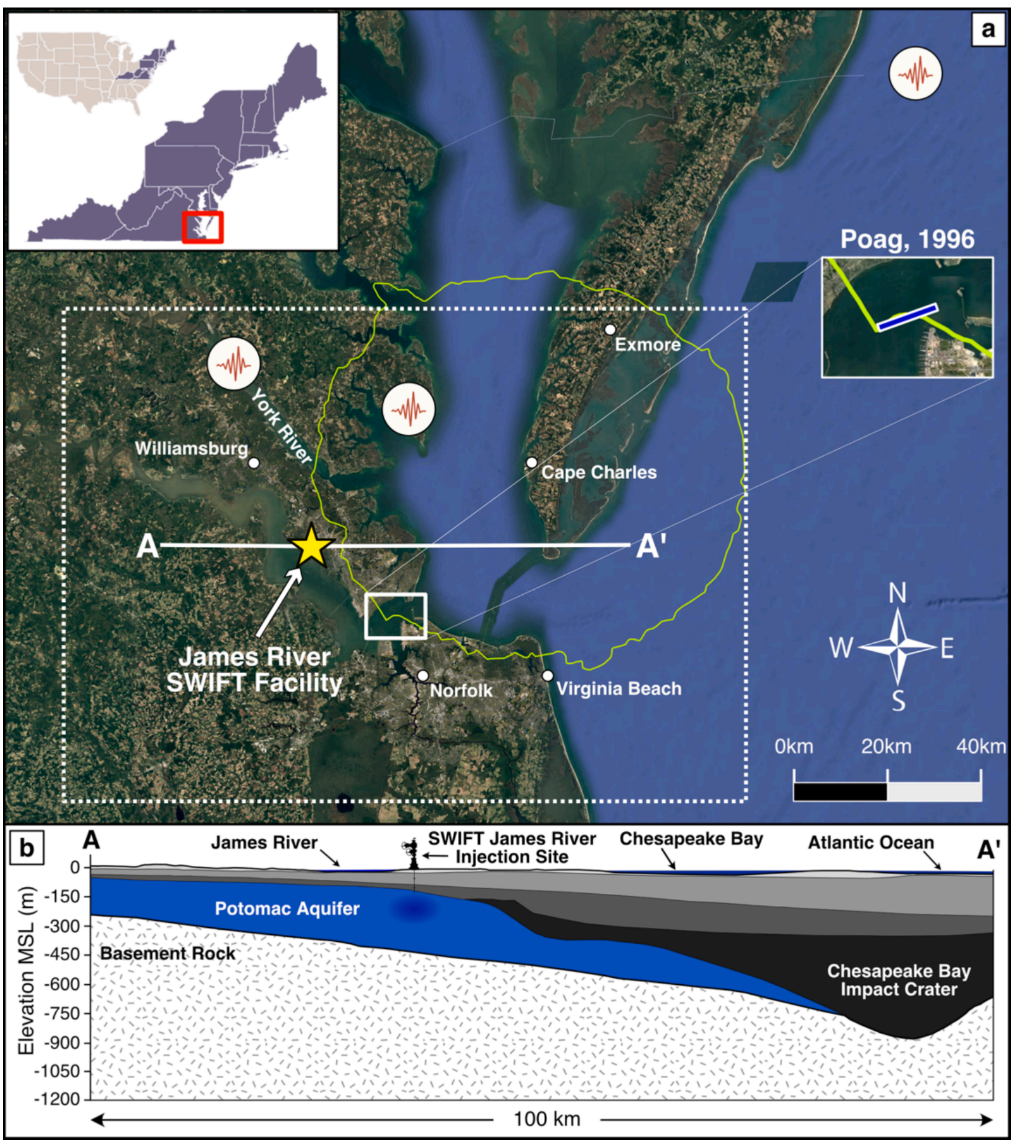

Fig. 1. A) Map of southeast Virginia. The star indicates the location of the James River Wastewater Treatment Plant – the first fully operational SWIFT site. The yellow polygon indicates the outermost most extent of the Chesapeake Bay Impact Crater. The seismic symbols within circles mark the approximate epicenter of the 1995 York River earthquake (~1 km depth; M2.9), February 2023 earthquake (~11 km depth; M2.6), and May 2024 earthquake (~8 km depth; M2.0). Line A-A' specifies the transect in Fig. 1B & 4. The blue line present in the zoomed window labeled Poag, 1996 indicates the extent of a 5 km interpreted seismic profile used for analysis in Fig. 7. The dashed box indicates the extent of the numerical simulations utilized in this research. B) Hydrogeologic cross-section from A-A', emphasizing geologic context for the Potomac Aquifer. (For interpretation of the references to colour in this figure legend, the reader is referred to the web version of this article.)

efforts, e.g., in the Hueco Bolson aquifer below El Paso, TX (Sheng and Devere, 2005), and the Floridian Aquifer below Punta Gorda, FL (Arthur et al., 2001), because the aquifer is in direct hydraulic communication with the underlying basement rock, which may be structurally weakened, as a result of Mesozoic rifting that occurred throughout the mid-Atlantic United States (Powars, 2000). Moreover, the SWIFT project is located on the flank of the Chesapeake Bay Impact Crater (CBIC), which formed approximately 35 million years ago, when a 3 to 5 km bolide collided with the continental shelf, carving out an 85 km wide by 1.3 km deep crater (Powars, 2000; Powars et al., 1993; Poag et al., 1994; Poag, 1996; Johnson et al., 1998; Powars, et al., 1999) (Fig. 1). The collision greatly disrupted pre-impact strata located within the study site, resulting in megablocks and faults that penetrate the basement rock surrounding the crater (Powars, 2000; Poag, 1996; Powars, et al., 1999).

While the basement rock underlying the Potomac Aquifer remains poorly characterized, the Langley Granite offers a rare glimpse into its composition (Horton et al., 2005). Identified at the NASA Langley Research Center in Hampton, Virginia, this granitoid body was sampled in the USGS-NASA Langley borehole at depths between 626.3 and 635.1 m. The core reveals a chloritized, weathered granite profile with a distinct nonconformity at its upper contact, overlain by Cretaceous Potomac Formation sediments. Seismic-reflection data suggest a weathering profile of approximately 40 m, offering detailed insights into the granite's composition and degree of alteration (Catchings et al., 2002). However, the Langley borehole represents a single data point in a region with sparse subsurface information. While it provides valuable details on the rock's weathering and textural characteristics, it cannot capture the full extent of heterogeneities or structural features, such as potential faulting, that may exist across the broader buried pluton.

Seismic-reflection studies of the Chesapeake Bay impact structure show that the coastal plain basement is disrupted by a mix of high-angle normal faults and low-angle reverse faults, though large portions of the basement appear relatively undisturbed (Catchings et al., 2002; Poag et al., 1999). A seismic profile from the area near the USGS-NASA Langley borehole reveals about 200 m of elevation change at the basement surface, accompanied by numerous diffractions. These diffractions suggest the presence of irregularities such as mineralized fractures and faults within the Langley Granite. While the seismic profile indicates faulting in the overlying sedimentary layers, likely caused by the late Eocene impact, the limited length of the granite core did not provide direct evidence of these faults (Catchings et al., 2002). Thus, the exact extent of faulting within the granite remains uncertain, although it is inferred that some faults may slightly offset the basement near the borehole.

Assessing the risk of injection-induced seismicity in the Virginia Coastal Plain is hampered by incomplete knowledge about presence of pre-existing faults in the region. Nevertheless, there are several lines of evidence to indicate that MAR activities may alter the regional seismicity rate. Specifically, the CBIC is known to be surrounded by ring faults, suggesting that a subset of these faults may be optimally aligned with the regional stress field and thus prone to reactivation. In terms of naturally occurring earthquakes, the United States Geological Survey Comprehensive Earthquake Catalog lists a magnitude-2.9 (M2.9) earthquake that occurred ~ 1 km below the York River in 1995, thus implying the presence of at least one seismogenic fault in the study area (Fig. 1). More recently, a M2.6 earthquake was recorded in offshore Virginia at ~ 11.2 km depth on February 8th, 2023, and a M2.0 occurred approximately 20 km east Gloucester, Virginia, on May 13, 2024 (Fig. 1). This latter earthquake, detected using the Hampton Roads Seismic Network (Pollyea et al., 2022), occurred at a depth of 8 km within the areal extent of the Chesapeake Bay Impact Crater. The seismograms are provided in Fig. S1, and SAC files from all stations are included in the electronic supplement to facilitate independent analysis. These natural earthquakes suggest that seismogenic faults may exist beneath the Virginia Coastal Plain, and in close proximity to the Chesapeake Bay Impact Crater.

To assess the potential for MAR activities in southeast Virginia to induce pore pressure transients that may result in unintended seismic activity, this study aims to quantify the extent and magnitude of fluid pressure propagation into the basement rock underlying the Potomac Aquifer during the SWIFT injection program at the James River WWTP (2026–2041). This analysis incorporates the planned injection rate of 61,000 m^3/day (16 M gpd) and considers the critical role of poorly constrained basement permeability. Basement rock permeability fundamentally influences the propagation of fluid pressure into the deep subsurface, with implications for seismic risk (Conley et al., 2022). Given these uncertainties, the study applies ensemble simulation methods to evaluate a range of permeability scenarios and provide probabilistic estimates of pressure propagation. This framework enables a comprehensive assessment of fluid pressure behavior in the basement rock and informs understanding of potential seismic hazards associated with future MAR operations.

2. Methods

Building on the objectives outlined in the introduction, this study employs a regional-scale numerical model to investigate fluid pressure transients caused by high-rate MAR operations. Ensemble simulation methods are implemented to address the uncertainty in basement rock permeability and to constrain the depth, extent, and magnitude of fluid pressure propagation. Specifically, the analysis involves: (i) developing 50 models with spatially random and equally probable permeability distributions within the basement rock, (ii) simulating the SWIFT injection scenario using a planned rate of 61,000 m^3/day (16 M gpd) across each model domain, and (iii) calculating e-type estimates to determine the mean and standard deviation of fluid pressure for each grid cell. Large-scale 3-D ensemble simulation is computationally expensive, so the decision to simulate an ensemble comprising 50 individual simulations reflects a balance between computational efficiency and generating sufficient simulation data to capture variability associated with a wide range of possible outcomes. Previous research indicates that simulation ensembles comprising 50 realizations provides robust underlying data for e-type estimation (Pollyea et al., 2014; Jayne et al., 2019; Koehn et al., 2023). For the present study, ensemble simulation results provide a probabilistic understanding of fluid pressure changes in the basement rock, enabling a detailed assessment of the potential for pressure-induced seismicity.

2.1. Model development

The study area is located in southeast Virginia (Fig. 1), where the SWIFT project is planning to come online at the James River WWTP in 2026. The study area comprises an extent of 170 km by 180 km. The geologic model developed for this study is based on the hydrostratigraphic framework for the Virginia Coastal Plain Aquifer System (Caldwell and McFarland, 2022), which includes the Upper Chesapeake Composite, Piney Point, Aquia, and Potomac aquifers and associated confining units (Fig. 2). The physical parameters for these layers are provided in Table S1. This framework is based on information from a network of 403 boreholes, with 129 of these located within our study area (Caldwell and McFarland, 2022). In addition, the geologic model comprises the complete areal extent and depth of the Chesapeake Bay Impact Crater, which is known to play a prominent role in the regional hydrogeologic system (Powars, 2000; Powars et al., 1993; Poag et al., 1994; Poag, 1996; Johnson et al., 1998; Powars, et al., 1999). Lastly, the geologic model comprises crystalline basement rock below the aquifer system to a maximum depth of 7.5 km below mean sea level. The geologic model is discretized into approximately ~ 732,500 grid cells using Voronoi tessellation in the horizontal plane and regular discretization with decreasing resolution in the vertical direction (Fig. S2). For each layer in the model domain, permeability, porosity, and compressibility for each stratigraphic layer are sourced from various

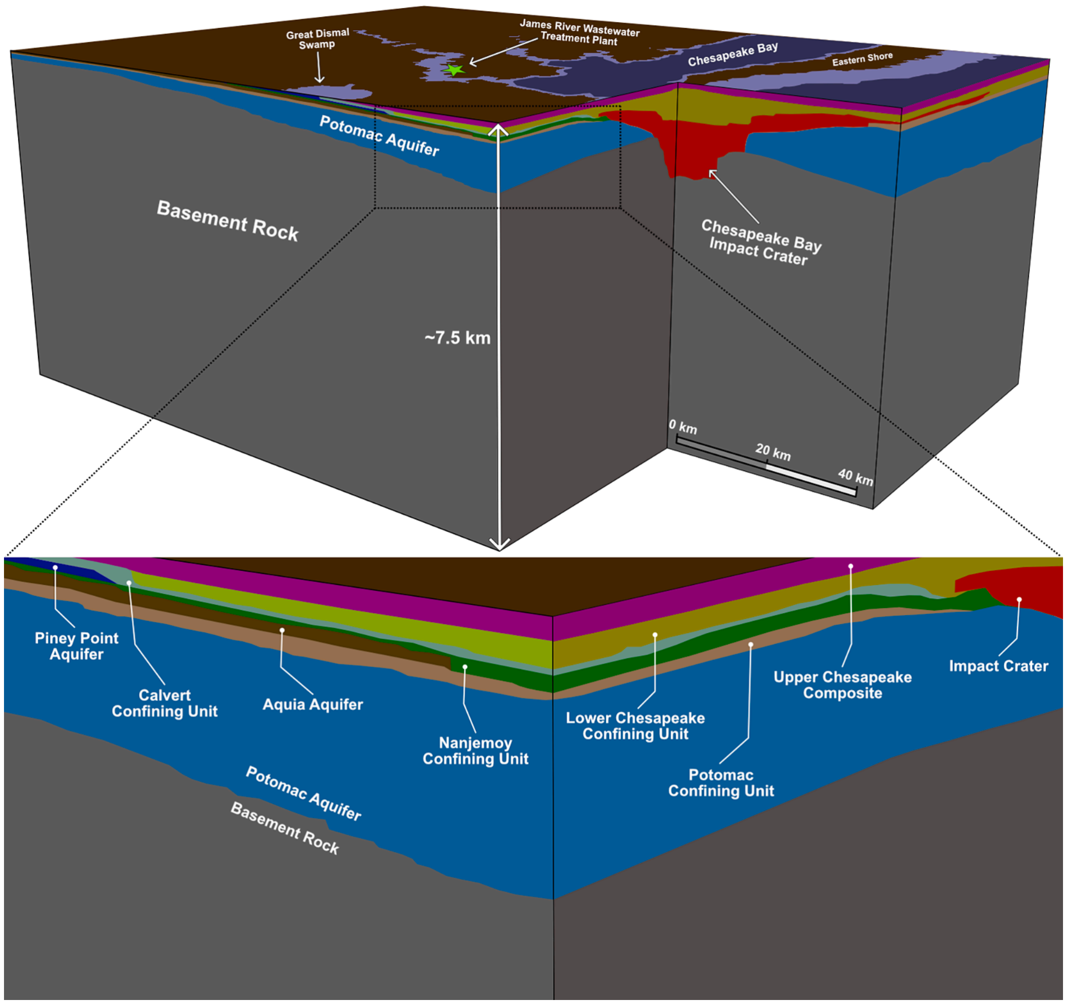

Fig. 2. The geologic model for this study, incorporating the established hydrostratigraphic framework for the Virginia Coastal Plain Aquifer System (Zhang et al., 2020).

references (McFarland and Scott, 2006; Heywood and Pope, 2009; Masterson et al., 2013) (Table S1), and basement permeability is discussed in greater detail below.

2.2. Basement rock permeability

Basement permeability plays a fundamental role in the timing and magnitude of fluid pressure propagation to seismogenic depths, e.g., $\geq\sim 2$ km. Nevertheless, permeability of the crystalline basement rock constitutes a significant source of uncertainty because it remains poorly understood in passive coastal margins. To address this uncertainty, this study implements ensemble simulation methods by generating fifty equally-probable basement permeability distributions for subsequent stochastic analysis. In doing so, fifty unique models are developed, each with identical aquifer properties, but randomly distributed effective permeability in the basement rock. Each basement permeability distribution is drawn at random from a normal distribution with a mean permeability of 1×10^{-14} m^2, based on values from Clauser (1992) (Clauser, 1992) and Manning & Ingebritsen (1999) (Manning and Ingebritsen, 1999), and a standard deviation of 7×10^{-15}. To account for the phenomenon in which deep basement permeability is known to decrease with increasing depth, each random distribution is then scaled according to the depth-dependent permeability ($k(z)$) model proposed by (Saar and Manga, 2004) (Fig. 3). In this formulation, $k(z)$ is calculated as a piece-wise function with exponential decay at depths less than 800 m and power law decay at depths greater than 800 m (Fig. 3) (Equation (1) (Saar and Manga, 2004).

$$K(z) = \begin{cases} K_s e^{-z/\delta} & z \leqslant 800\,\text{m} \\ K_d \left(\frac{z}{d}\right)^{-3.2} & z > 800\,\text{m} \end{cases} \tag{1}$$

This formulation incorporates several parameters: k_s represents near-surface permeability, δ is a fitting parameter with a fixed value of 800 m in this model, and k_d denotes the permeability at depth d, where the transition occurs from exponential decay to power law decay (specifically, $k_d = k(800\ m)$). Equation (1) was applied to all grid cells within the basement subdomain, with the initiation of permeability decay taking place at the boundary between the basement rock and the Potomac aquifer. This process is visually depicted in Fig. 3. Each of the fifty depth-dependent basement permeability models is characterized by a k_s parameter, which represents the permeability value at the start of the depth-decay process (i.e., the permeability of the first basement cell in each model). This approach encompasses permeability variations within the basement rock, while also enabling for the ability to run multiple random iterations, enhancing suitability for uncertainty analysis which is critical for accurately predicting pore pressure propagation during high-rate fluid injections.

2.3. Initial conditions

Groundwater within the study area comprises a complex assemblage of low-, moderate-, and hyper-saline waters (Johnson et al., 1998; Poag,

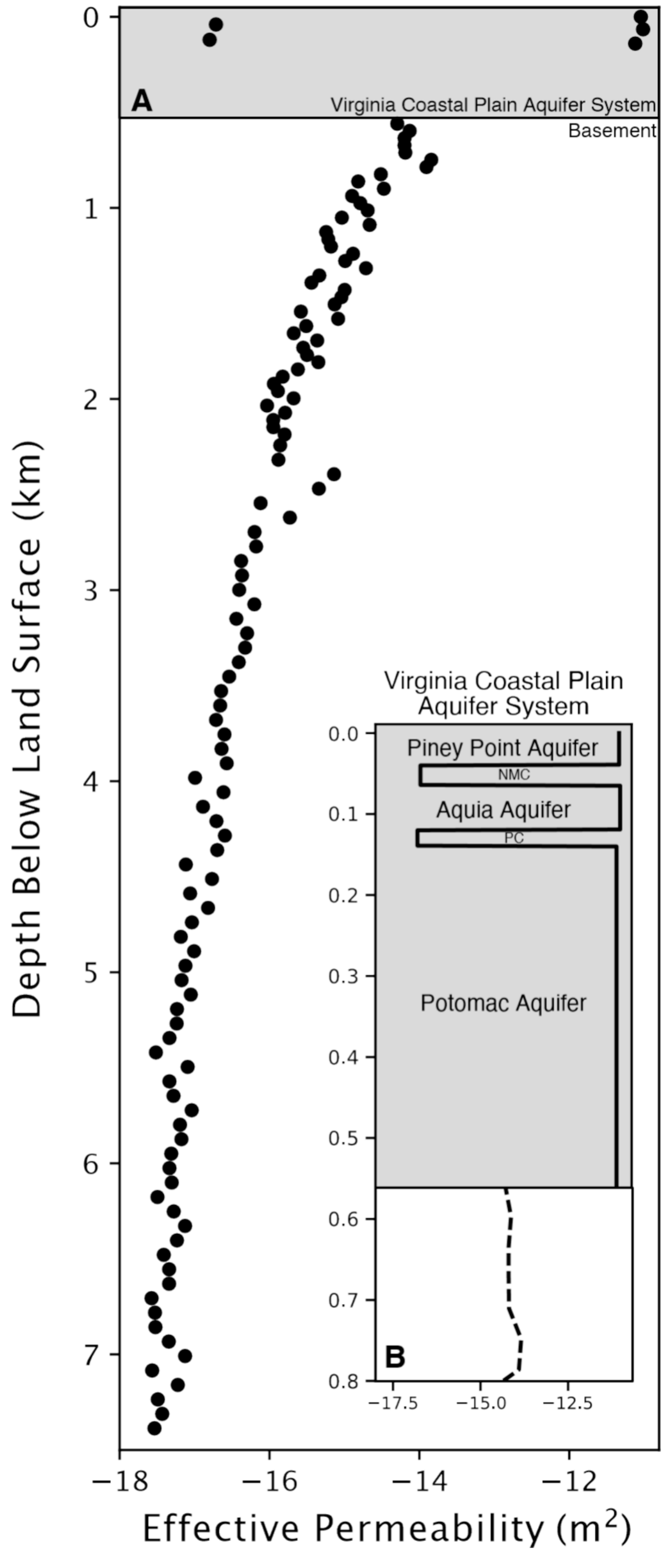

Fig. 3. A) The average effective permeability profile, derived from 50 Monte Carlo realizations beneath the James River injection site, uses randomly assigned basement rock permeability values from a normal distribution with a depth-dependent decay function. This is not observed data. B) The Virginia Coastal Plain Aquifer is indicated by grey shading and is expanded for a detailed view. Areas of high permeability indicate aquifer sediments, including the Piney Point, Aquia, and Potomac Aquifers and areas of low permeability indicate confining units, including the Nanjemoy Marlboro (NMC) and Potomac (PC) Confining Unit.

1998). Aquifers underlying the land surface comprise low salinity groundwater that forms the basis for water resources within the study area; whereas, offshore aquifers and deep basement rocks are generally comprised of moderately saline groundwater with composition similar to seawater. Hyper-saline waters occur within the sediments that fill the Chesapeake Bay impact crater (Poag, 1998). To accurately represent these complexities, generating initial conditions for this study requires preliminary simulations aimed at achieving (i) geochemical, pressure, and temperature equilibrium and (ii) a realistic depiction of current aquifer conditions. First, the geochemical equilibrium is attained by delineating three distinct initial groundwater salinity regions, pure freshwater (1000 kg/m^3), pure seawater (1024 kg/m^3), and hyper-saline water within the Chesapeake Bay impact crater (1042 kg/m^3). This initial simulation imposed surface boundary conditions comprising mean annual surface and seafloor temperatures, where applicable, as well as a basal heat flux of (65 mW/m^2). This initial simulation was run to steady-state, resulting in a hydrostatic pressure gradient with thermal and geochemical equilibrium throughout the model domain. Second, results from the equilibration run were used as initial conditions for a spin-up simulation to estimate pressure and temperature conditions within the aquifer system in year 2026, when SWIFT MAR operations are scheduled to come online. In doing so, the spin-up run accounts for 44 years (1982——2026) of groundwater withdrawals throughout the study area using groundwater well production data from 1982 to 2019, which were provided by Virginia Department of Environmental Quality (VDEQ). In order to simulate groundwater withdrawals through 2026, the spin-up run reproduces 2019 withdrawal rates from 2020 to 2026. Mean annual groundwater withdrawals are illustrated in Fig. S3. The results of this spin-up run form the initial conditions to forward model SWIFT MAR injection operations.

2.4. Numerical simulation

The injection scenario for this study comprises the MAR operations that are planned for the SWIFT James River Wastewater Treatment Plant (JR WWTP), which will recharge the Potomac Aquifer a rate of 61,000 m^3 per day (16 M gpd) beginning in 2026. Within this context, the JR WWTP injection scenario is reproduced within each of the fifty model domains for a period of 15 years (2026——2041). Groundwater extraction rates are assumed to remain constant at 2019 levels for the duration of the simulation, as no extraction data are available beyond that year.

2.5. Code selection

The code selection for this study is TOUGH3 (Jung et al., 2017) compiled with EOS7, which is the equation of state module for non-isothermal mixtures of water, brine, and air. TOUGH3 solves energy and mass conservation equations for non-isothermal multiphase flows in porous geologic media, while the EOS7 module internally calculates fluid properties as a function of pressure, temperature and composition (i.e., PTX dependence). Within this simulation framework, the EOS7 module is suitable for problems involving multiphase, density-driven flows where salinity does not reach saturation levels. The TOUGH3 simulator utilizes integral finite volume discretization in space and first-order finite differences in time. Additional details about code selection and governing equations are provided in the Electronic Supplement that accompanies this manuscript.

2.6. Data analysis

To assess the extent and magnitude of injection-induced pressure transients after 15-years of MAR operations at JR WWTP, the fluid pressure change (ΔP) throughout each grid cell of each model is calculated as,

$$\Delta P = P(t_i) - P(t_\circ) \quad (2)$$

where, $P(t_i)$ is the fluid pressure in any given grid cell at a specified time of injection t_i and $P(t_o)$ is the initial fluid pressure within a grid cell. The ΔP for the complete ensemble of 50 simulations is analyzed using e-type methods (Deutsch, 1999); which calculate the mean and standard deviation for each grid cell at each *x,y,z* location within the model domain. This method consolidates the fifty individual simulations into a single representation, providing the mean fluid pressure change and the standard deviation for each grid cell. In doing so, the e-type method provides a measure of simulation uncertainty that may be a useful metric to guide operational decision-making.

3. Results and discussion

3.1. High-Rate MAR Drives pressure into basement

Previous research suggests that increasing fluid pressure by 10 to 70 kPa may be sufficient to induce earthquakes on pre-existing faults that are critically stressed and favorably aligned with the regional stress field (Reasenberg and Simpson, 1992; Keranen et al., 2014). Consequently, this study adopts a conservative threshold of 40 kPa as the lower bound for fluid pressure change that may be required to induce earthquakes within the study area. Simulation results show that MAR activities planned for the James River SWIFT site are likely to increase fluid pressure above 40 kPa throughout a substantial volume of basement rock below the Potomac Aquifer (Figs. 4 & 5). The mean 40 kPa contour reaches a maximum depth of 3 km immediately below the injection site, while the 3σ confidence interval ranges from Nevertheless, permeability of the crystalline ~ 2.7 to 3.7 km depth (Fig. 4). This suggests that fluid pressure transients capable of causing injection-induced earthquakes are likely to reach seismogenic depths within 15 years of MAR operations at the James River SWIFT site. To assess the lateral extent of fluid pressure propagation within the basement rock, Fig. 3 presents horizontal slices through the model domain at 1 km, 2 km, and 3 km, which illustrate that (i) the magnitude of pressure change increases in concentric rings immediately below the injection site and (ii) the lateral extent of pressure change is greatest at shallow depths with a maximum radial extent of ~ 53 km at 1 km depth and ~ 25 km at 3 km depth. The lateral extent of the 40 kPa pressure front reaches its maximum in the direction of the

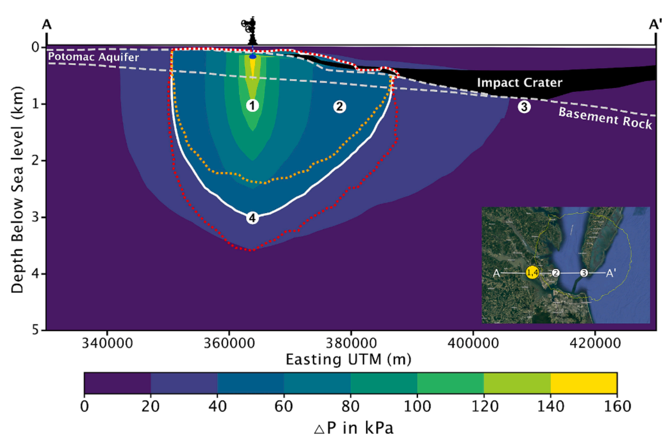

Fig. 4. Two-dimensional cross-section view (5x vertical exaggeration) through the SWIFT James River Injection Site from A to A' (Fig. 1) with contours of fluid pressure generated by 15 years of injections at a rate of 16 M gpd. The colored contours represent the average ΔP from injections. The white contour line indicates the average 40 kPa ΔP contour, while the dotted red and orange lines represent the + 3σ and −3σ standard deviation confidence 40 kPa ΔP contour for all fifty simulations, respectfully. The small blue symbol below the injection well icon is the approximate interval of injection. Numbers 1–4 indicate the locations for data presented in Fig. 6. (For interpretation of the references to colour in this figure legend, the reader is referred to the web version of this article.)

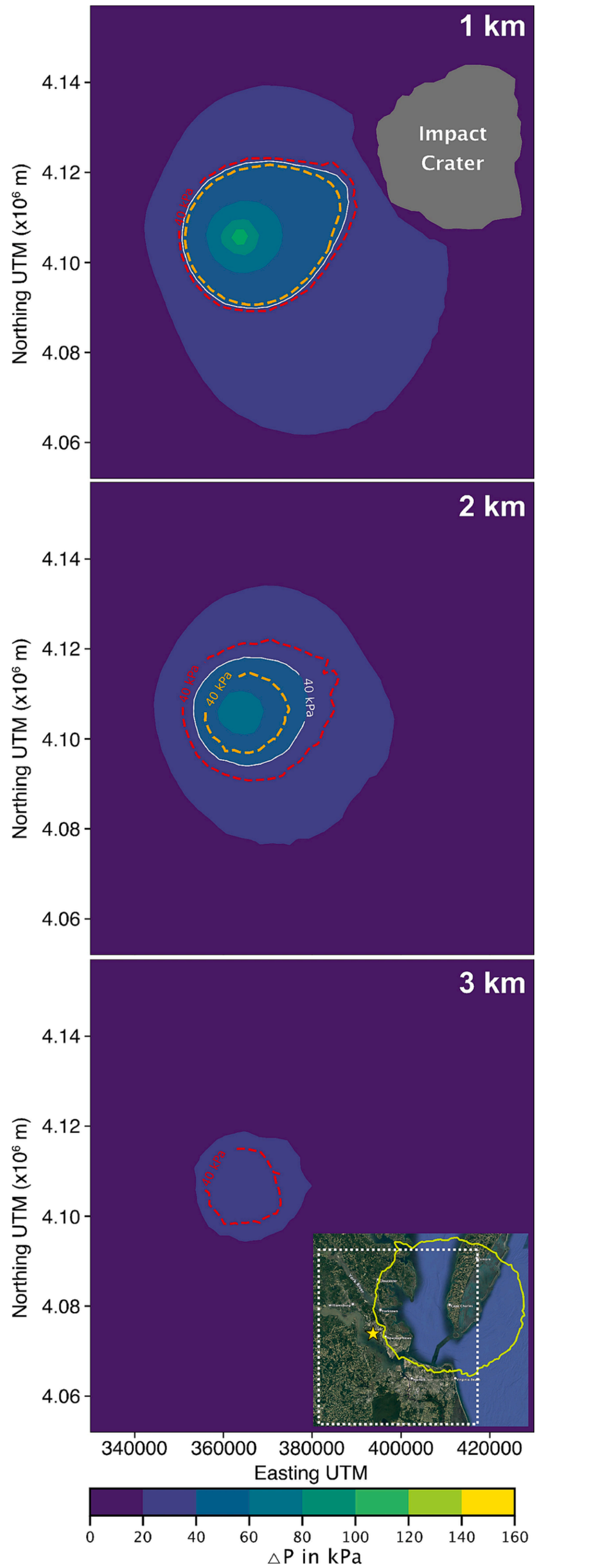

Fig. 5. Plan view slices at depths of 1 km, 2 km, and 3 km provide regional context for changes in fluid pressure after 15 years of injections at the James River SWIFT site. The dotted box present in the site map inlay indicates the spatial extent of each panel. The colored contours represent the average ΔP from injections. The white contour line indicates the average 40 kPa ΔP contour, while the dotted red and orange lines represent the + 3σ and −3σ standard deviation confidence 40 kPa ΔP contour for all fifty simulations, respectfully. (For interpretation of the references to colour in this figure legend, the reader is referred to the web version of this article.)

CBIC because the crater is comprised of low permeability tsunami deposits that back-filled the crater after impact (Powars, 2000). Consequently, the crater is generally considered to be a hydraulic barrier, which when combined with the eastward structural gradient, causes fluid pressure to accumulate at the crater rim. Because the basement rock surrounding the crater rim is known to be surrounded by rim faults (Poag et al., 2012), this region may be particularly susceptible to MAR-induced seismicity.

3.2. Potential for induced seismicity

Fluid pressure transients capable of inducing seismic activity are likely to reach seismogenic depths within 15 years of MAR injections at the SWIFT James River facility. To assess the temporal variations of these pressure transients, Fig. 4 illustrates time series simulation data for pressure change (ΔP) at four monitoring locations within the basement (Fig. 4, white numbered circles). The results show that pressure change is most pronounced near the injection site. Specifically, monitoring locations 1 and 2 experience rapid pressurization, exceeding 40 kPa within two and four years, respectively, before stabilizing to a slower, steady increase. This suggests that induced seismic activity could occur within the first two years of MAR operations, provided basement faults are present in the pressurized rock. In contrast, monitoring locations 3 and 4 show a more gradual, linear pressure increase, with ΔP surpassing 40 kPa only at location 4. In terms of model variability, Fig. 4 presents the complete ΔP envelope (blue shading) for all 50 simulations at each monitoring location. This envelope shows that the ΔP range is much larger (10 – 25 kPa) at monitoring locations 1 and 4, while the ΔP variability at monitoring locations 2 and 3 only ranges by 0—–3 kPa. These results imply that model uncertainty is greatest directly beneath the injection site, regardless of the depth (locations 1 and 4). In contrast, the modeled pressure changes at larger radial distances from the injection site (locations 2 and 3) exhibit much lower variability, regardless of pressure magnitude. This reduced variability is largely driven by the spatially variable basement permeability distributions used in the model. These results highlight the significant role of permeability in determining pressure propagation. While pressure changes at distant locations stabilize more consistently, the variability in pressure predictions near the injection site is much more sensitive to changes in permeability. Therefore, obtaining tighter constraints on basement permeability, particularly below the injection site, is crucial for reducing model uncertainty and improving the accuracy of pressure predictions. Enhanced permeability data from the injection zone would allow for a more precise characterization of pressure propagation, which is critical for assessing the potential for injection-induced seismicity and optimizing pressure management strategies.

Simulation results illustrate that fluid pressure transients from MAR injections at the James River WWTP site are likely to reach seismogenic depths within the bounds of permeability uncertainty tested here. Moreover, these results show that MAR-induced pressure transients are likely to interact with low permeability CBIC sediments and surrounding structural irregularities, which were discovered by a 2-D seismic reflection survey in Poag (1996) (Poag, 1996). The location of this survey occurs ~ 15 km southeast of the James River SWIFT facility (Fig. 1), and the survey reveals the presence of rim faults, compaction faults, and slumped megablocks within impact crater sediments, as well as highly deformed basement rock. Since the impact, the region has remained tectonically stable (Collins and Wünnemann, K. , 2005); however, these features are zones of crustal weakness and have the potential for continued slow movement, or sudden offsets if reactivated by pressure transients (Poag, 1998). In this context, Fig. 5 illustrates simulated fluid pressure change within the cross-section previously imaged in Poag (1996) (Poag, 1996). This analysis shows that MAR activities at the James River SWIFT site may drive fluid pressure transients of 30 to 40 kPa into structural weaknesses within the impact crater and upper basement rock after 15 years of MAR activities. While these pressure magnitudes fall within the lower range of the threshold for inducing seismic activity, there remains substantial uncertainty about the nature and effects of interactions between injection-induced pressure transients and buried impact crater structures.

3.3. Pressure management strategies

While it is widely accepted that fluid pressure transients ranging from 10 to 70 kPa can trigger earthquakes on critically stressed, optimally oriented faults, recent research suggests that the rate of pressure change (pressurization rate) may be an even more critical factor than pressure magnitude in the onset of injection-induced earthquakes (Alghannam and Juanes, 2020). Alghannam and Juanes (2020) further suggest that injection strategies designed to decrease the pressurization rate (dP/dt) are critical for mitigating the seismic risk associated with industrial-scale subsurface fluid injections (Alghannam and Juanes, 2020). The basement pressurization rate (dP/dt) for the James River SWIFT site is shown in Fig. 6A for a single simulation at monitoring location 1. For this injection scenario, the injection rate comes on instantaneously at 61,000 m^3/day (Fig. 6A, dashed black line) and results show that the sudden initiation of injections at 16 M gpd creates a dramatic spike in rate of fluid pressure change before rapidly declining (Fig. 6A, solid black line). This rapid increase of pressurization rate is shown to intensify fault destabilization (frictional sliding) in early-time, thus increasing the potential for an induced-earthquake to occur (Alghannam and Juanes, 2020).

To mitigate this rapid change in pressurization rate, we tested three injection strategies that gradually increase the injection rate to the desired target rate over a 12-month period. The three injection strategies comprise: (i) linear increase, (ii) exponential growth, and (iii) exponential decay (Fig. 6, dashed lines). For all three injection strategies, a gradual increase in the injection rate results in a substantially lower pressurization rate than the case when the injection rate is applied instantaneously. Moreover, this analysis shows that the linearly increasing injection rate provides the greatest reduction in pressurization rate (Fig. 6A); in fact, the linear injection rate strategy yields ~ 66 % decrease in pressurization rate in comparison to the original scenario (Fig. 6A, solid gray line). Moreover, the linear injection rate strategy (Fig. 6A, gray) injects more water into the aquifer over the 12-month ramp-up period than the exponential growth injection rate strategy (Fig. 6, blue), while maintaining a lower pressurization rate. And while the exponentially decreasing injection rate strategy and original scenario inject more water into the aquifer than the linear injection over the 12-month ramp-up period, this comes at the expense of much greater pressurization rates. In addition, the maximum magnitude of fluid pressure change after 15 years is the same for all four injection strategies (Fig. 6B); however, the maximum fluid pressure is achieved asymptotically at varying times for each injection strategy. As a result, this analysis strongly implies that the linear injection rate ramp-up is an optimal injection strategy for maximizing aquifer recharge volume and minimizing pressurization rate, while simultaneously achieving the long-term pore pressure that is required to mitigate land subsidence and saltwater intrusion in the Potomac Aquifer.

To underscore the broader applicability of this work, these findings represent an initial step toward the development of guidelines for managing pressure in high-rate MAR operations. While further data from full-scale operations is needed to establish comprehensive recommendations, this study highlights the possible importance of ramp-up injection strategies as a practical approach for mitigating seismic risks in MAR projects globally.

The Virginia Coastal Plain is a passive coastal margin where a thick sediment package, comprising the Potomac Aquifer, is juxtaposed unconformably on transitional basement rock sloping toward oceanic crust (Erskine and Vail, 1987; Steckler et al., 1993). This geologic configuration is widespread globally (Fig. 9), where, in many cases, the deepest stratigraphic layer features a viable freshwater aquifer with direct

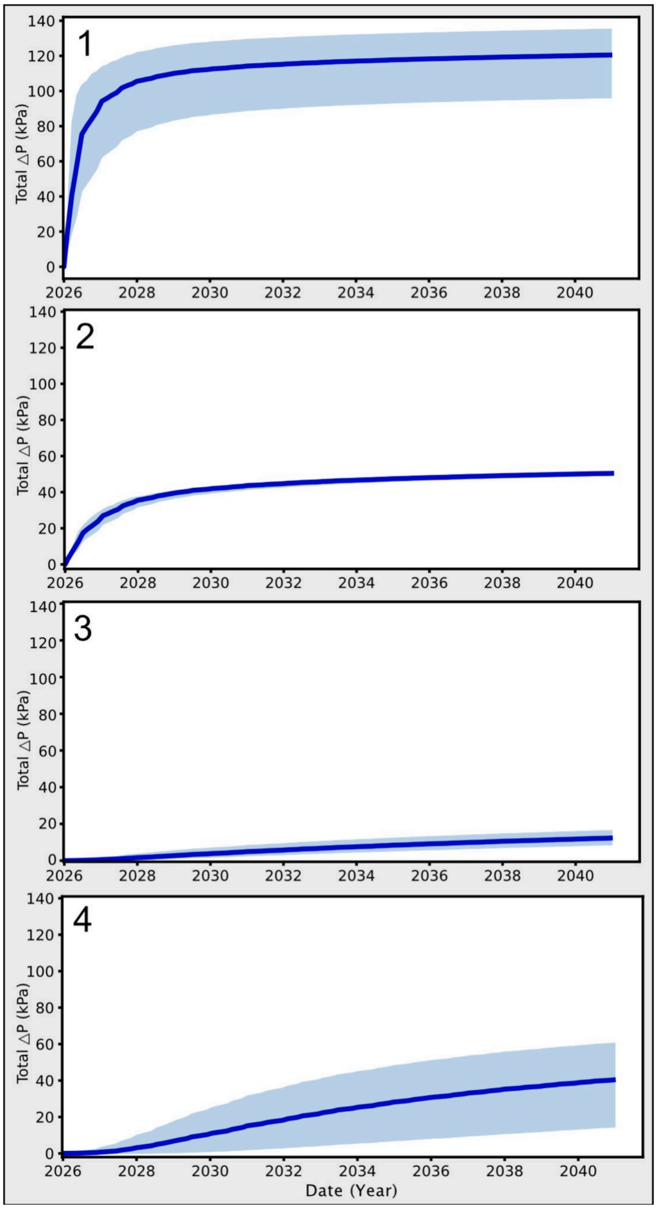

Fig. 6. Absolute ΔP values for four locations in the study area. Locations 1, 2, & 3 are located at 1 km depth, while location 4 is located at 3 km depth. All four locations are further indicated in Fig. 4. Solid lines represent the average from Monte Carlo simulations while the shaded buffers represent the minimum and maximum values at each location.

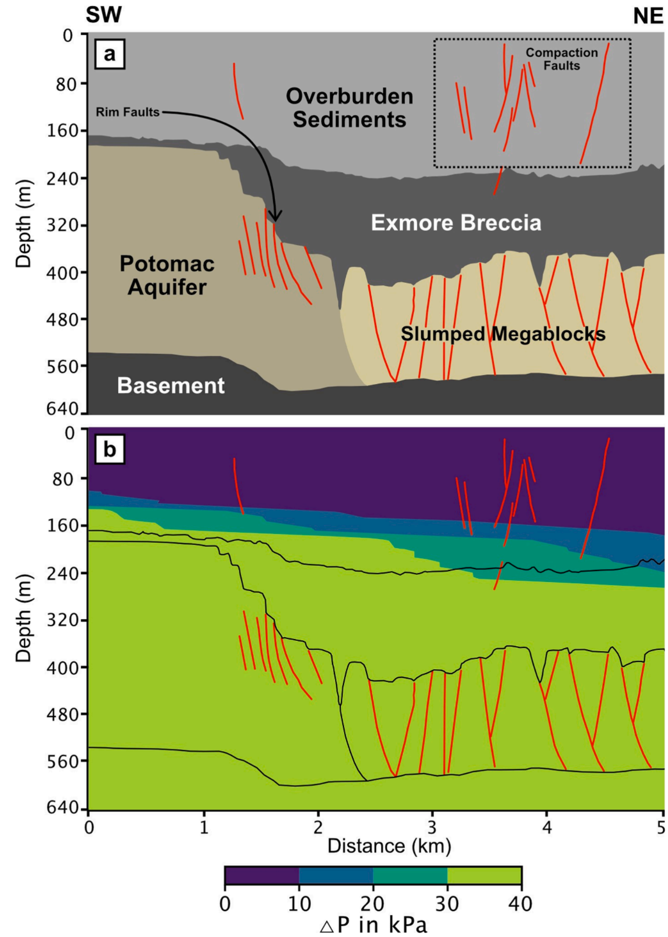

Fig. 7. A) Interpreted seismic data from (Jayne et al., 2019), showing features associated with the CBIC including rim faults, compaction faults, and slumped megablocks. Location of seismic profile indicated in Fig. 1. b) ΔP values after 15 years of injection at the James River SWIFT site overlain on CBIC features.

hydraulic communication with the underlying crystalline basement. Observations from the Gravity Recovery and Climate Experiment (GRACE) have revealed that among Earth's 37 largest aquifers, 10 are experiencing both variable degrees of aquifer stress, surpassing sustainability thresholds, and partially intersect with a passive coastal margin (Richey et al., 2015) (Fig. 9). Using the categorization outlined by Richey et al. (2015) (Richey et al., 2015), four of these ten aquifers are overstressed (Fig. 7A, red), while six are categorized as variably stressed (Fig. 7A, blue).

The (Fig. 8) SWIFT project addresses aquifer stress in the Potomac Aquifer, which is situated within the Atlantic and Gulf Coastal Plains Aquifer System and shares a similar hydrostratigraphic context with the Ogaden-Juba Basin, the Canning Basin, and the Nubian Aquifer System. The Ogaden-Juba Basin has long been a vital source of groundwater for East African populations (Quiroga et al., 2022). These East African regions face water scarcity due to low precipitation, high evapotranspiration, and contamination of shallow water resources found at depths less than 400 m (Quiroga et al., 2022; Fao-swalim, 2012). Depletion of shallow aquifers has prompted investigations into deeper groundwater sources, including the Adigrat Formation, which is known to contain fresh water (Purcell, 1979) and sits unconformably above the basement rock (Fig. 7a). Although the Adigrat Formation remains largely untapped, there is potential for this region to rely on it for significant groundwater supplies. To prevent or mitigate potential depletion of the Adigrat Formation, high-rate MAR represents a viable option. However, given the stratigraphic geometry of the Adigrat Formation, seismic activity could emerge as a future concern, necessitating pressure management strategies to ensure sustainable water management practices.

The Canning Basin in Western Australia provides freshwater for domestic, agricultural, and mining activities. GRACE data has revealed a net decline in groundwater storage within the Canning Basin (Richey et al., 2015), potentially linked to iron ore mining or climate-related factors (Richey et al., 2015; Opie et al., 2020; Munier et al., 2012). It is becoming increasingly likely that this arid region may soon need to rely on deeper freshwater sources, such as the Wallall Aquifer (Fig. 7b), which is extensively confined, and remains largely untapped (Government of Western Australia., 2012). The Wallall Aquifer also directly overlays the crystalline basement. If this confined reservoir is to be utilized, strategies like high-rate MAR may be necessary to prevent further depletion, thus carrying the associated risk of inducing seismic activity.

The Nubian Aquifer System spans northeastern Africa, providing

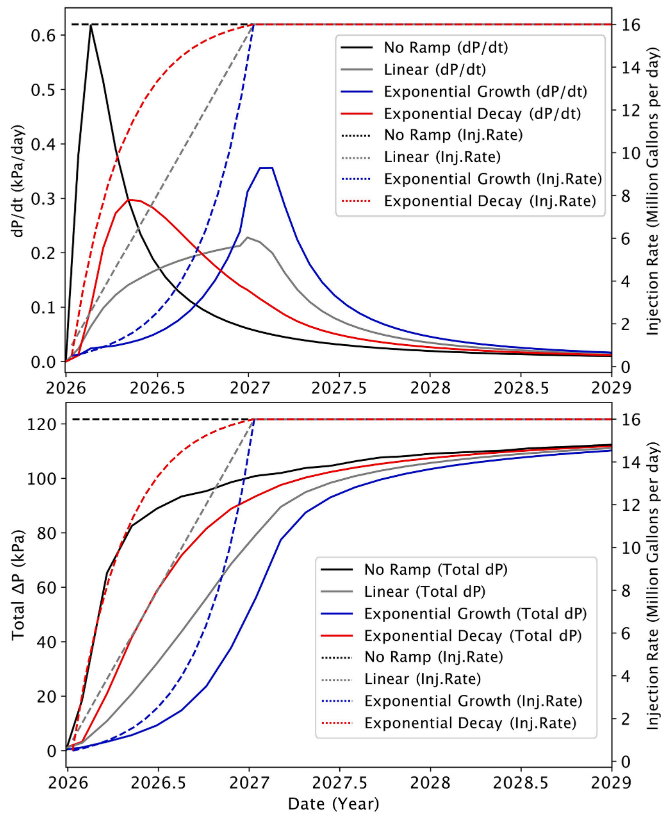

Fig. 8. In the top graph, rates of fluid pressure change (dP/dt) are displayed as solid lines for four different injection rate scenarios. Injection rates are displayed as dotted lines. In the bottom graph, absolute fluid pressure changes (ΔP in kPa) are displayed as solid lines for the same four injection rate scenarios as the top figure.

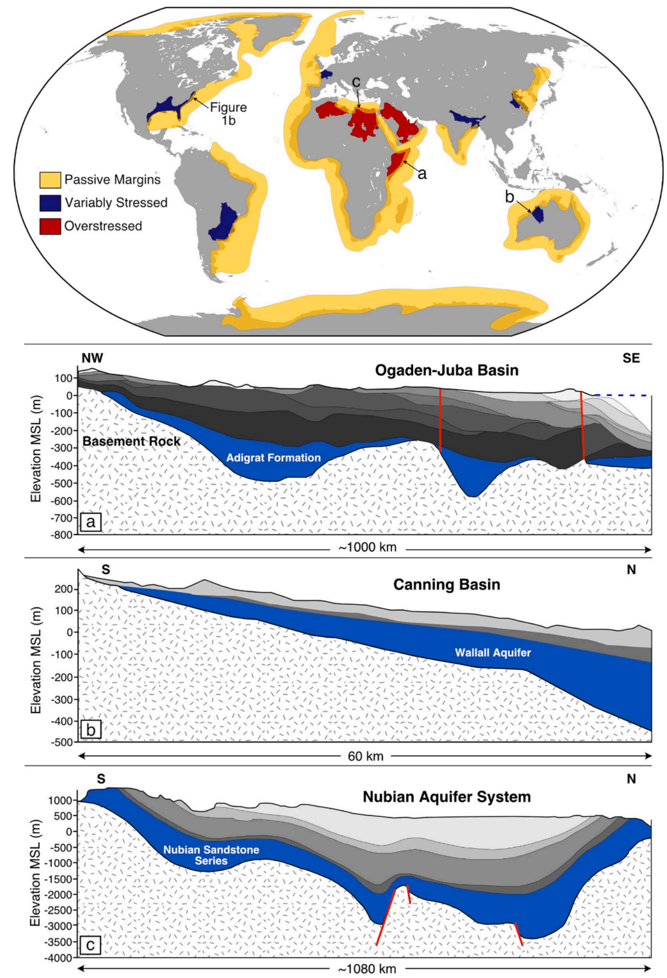

Fig. 9. Map showing the spatial relationship between passive margins (Munier et al., 2012) and variably stressed and overstressed aquifers (as defined in (Poag et al., 2012). Cross-sections a, b, and c display stratigraphic geometry of the Ogaden-Juba Basin, Canning Basin, and Nubian Aquifer System. The Adigrat Formation, Wallall Aquifer, and Nubian Sandstone Series serve or could potentially serve as deep freshwater aquifers. All three aquifers rest unconformably on crystalline basement rock.

crucial freshwater resources shared among Egypt, Sudan, Chad, and Libya (Ebraheem et al., 2002; Ebraheem, 2003; Ebraheem et al., 2003; Ebraheem et al., 2004; Voss and Soliman, 2014; Sefelnasr et al., 2015). Over-exploitation could cause shallow wells to run dry, presenting the need to seek deeper water sources (Voss and Soliman, 2014). Deep in the Nubian Aquifer System, the Nubian Sandstone Series, lying unconformably on crystalline basement rock, serves as an excellent source for fresh groundwater resources (Sefelnasr et al., 2015) (Fig. 7c). The amount of water extracted from the Nubian Aquifer System is projected to double over the next 50–100 years. Climate change will further stress the system (Sefelnasr et al., 2015), underscoring the potential need for strategies like high-rate MAR, which, while beneficial, must be carefully managed to mitigate risks and ensure long-term sustainability.

4. Conclusions

High-rate MAR is an important engineered solution to aquifer stress worldwide; however, passive coastal margins present unique challenges when the stressed aquifer sits unconformably above crystalline basement rock. In this study, numerical simulations reveal that MAR injections at 61,000 m^3/day into the variably stressed Potomac Aquifer can generate fluid pressure transients with sufficient magnitude to cause injection-induced seismicity. Despite this finding, however, the actual risk of injection-induced seismicity remains uncertain in the Virginia Coastal Plain because little is known about the presence and stress-state of seismogenic faults in the underlying basement. The results of this study show that pressure management strategies, such as gradually ramping up the injection rate, can reduce the pressurization rate. This approach helps mitigate the potential for injection-induced seismicity while still meeting the pressure objectives for the Potomac Aquifer. In a global context, this study shows that the hydrogeologic conditions within the Virginia Coastal Plain occur in variably and overstressed aquifers worldwide, and, as a result, the pressure management strategies described here offer a roadmap towards risk-aware methodologies for safeguarding groundwater resources and enhancing the resiliency of global communities.

CRediT authorship contribution statement

Ethan W. Conley: Writing – review & editing, Writing – original draft, Visualization, Validation, Software, Methodology, Investigation, Formal analysis, Conceptualization. **Cameron R. Chambers:** Methodology, Investigation, Conceptualization. **John B. Ogunleye:** Writing – review & editing, Visualization, Methodology, Investigation. **Lars W. Koehn:** Writing – review & editing, Methodology. **Dan Holloway:** Writing – review & editing, Resources, Project administration, Funding acquisition, Conceptualization. **Jamie Heisig-Mitchell:** Writing – review & editing, Resources, Project administration, Funding acquisition, Conceptualization. **Martin Chapman:** Validation, Project administration, Methodology, Investigation, Conceptualization. **Mahesh Parija:** Writing – review & editing. **Ryan M. Pollyea:** Writing – review & editing, Writing – original draft, Supervision, Resources, Project administration, Methodology, Investigation, Funding acquisition, Formal analysis, Conceptualization.

Declaration of competing interest

The authors declare that they have no known competing financial interests or personal relationships that could have appeared to influence the work reported in this paper.

Acknowledgements

This material is based in part upon work supported by the National Science Foundation under Grant Number 1735139. Any opinions, findings, and conclusions or recommendations expressed in this material are those of the authors and do not necessarily reflect the views of the National Science Foundation.

Appendix A. Supplementary data

Supplementary data to this article can be found online at https://doi.org/10.1016/j.jhydrol.2025.132767.

Data availability

Data will be made available on request.

References

Casanova, J., Devau, N., Pettenati, M., 2016. Managed aquifer recharge: an overview of issues and options. Integrat. Groundwater Manage. 413–434.
Gleeson, T., Wada, Y., Bierkens, M.F., Van Beek, L.P., 2012. Water balance of global aquifers revealed by groundwater footprint. Nature 488 (7410), 197–200.
Ringleb, J., Sallwey, J., Stefan, C., 2016. Assessment of managed aquifer recharge through modeling—A review. Water 8 (12), 579.
Dillon, P., Pavelic, P., Palma Nava, A., Weiping, W., 2018. Advances in multi-stage planning and implementing managed aquifer recharge for integrated water management. Sustainable Water Resour. Manage. 4 (2), 145–151.
Zhang, H., Xu, Y., Kanyerere, T., 2020. A review of the managed aquifer recharge: Historical development, current situation and perspectives. Phys. Chem. Earth, Parts a/b/c 118, 102887.
Conley, E., Chambers, C. R., Heisig-Mitchell, J., Holloway, D., and Pollyea, R. M. (2022). Utilizing numerical simulation to understand the implications of injection-induced seismicity for managed aquifer recharge in coastal Virginia. In OCEANS 2022, Hampton Roads, pages 1–8. IEEE.
Dillon, P., Stuyfzand, P., Grischek, T., Lluria, M., Pyne, R., Jain, R., Bear, J., Schwarz, J., Wang, W., Fernandez, E., et al., 2019. Sixty years of global progress in managed aquifer recharge. Hydrgeol. J. 27 (1), 1–30.
Pollyea, R., Chapman, M., Chambers, C., Conley, E., Holt, M., Mitchell, J., and Holloway, D. (2022). Introducing the Hampton Roads Seismic Network: Minimizing the Risk of Injection-Induced Seismicity in Virginia. OCEANS Conference 2022 Hampton Roads.
NRC (2013). Induced Seismicity Potential in Energy Technologies. National Academies Press, Washington D.C. U.S. National Research Council (NRC) Committee on Induced Seismicity Potential in Energy Technologies.
Ellsworth, W.L., 2013. Injection-induced earthquakes. Science 341 (6142), 1225942.
Weingarten, M., Ge, S., Godt, J.W., Bekins, B.A., Rubinstein, J.L., 2015. High-rate injection is associated with the increase in US mid-continent seismicity. Science 348 (6241), 1336–1340.
Ellsworth, W.L., Llenos, A.L., McGarr, A.F., Michael, A.J., Rubinstein, J.L., Mueller, C.S., Petersen, M.D., Calais, E., 2015. Increasing seismicity in the US midcontinent: Implications for earthquake hazard. Lead. Edge 34 (6), 618–626.
Pollyea, R.M., Chapman, M.C., Jayne, R.S., Wu, H., 2019. High density oilfield wastewater disposal causes deeper, stronger, and more persistent earthquakes. Nat. Commun. 10 (3077), 1–10.
Pollyea, R.M., Fairley, J.P., Podgorney, R.K., McLing, T.L., 2013. A field sampling strategy for semivariogram inference of fractures in rock outcrops. Stoch. Env. Res. Risk A. 27 (7), 1735–1740.
Saar, M.O., Manga, M., 2003. Seismicity induced by seasonal groundwater recharge at Mt. Hood, Oregon. Earth Planet. Sci. Lett. 214 (3–4), 605–618.
Ge, S. and Saar, M. O. (2022). Induced Seismicity During Geoenergy Development—A Hydromechanical Perspective. J. Geophys. Res.: Solid Earth, 127(3): e2021JB023141.
Zoback, M.D., Hickman, S., 1982. In situ study of the physical mechanisms controlling induced seismicity at Monticello Reservoir, South Carolina. J. Geophys. Res. Solid Earth 87 (B8), 6959–6974.
Brown, M.R., Ge, S., 2018. Small earthquakes matter in injection-induced seismicity. Geophys. Res. Lett. 45 (11), 5445–5453.
Pollyea, R.M., Mohammadi, N., Taylor, J.E., Chapman, M.C., 2018. Geospatial analysis of Oklahoma (USA) earthquakes (2011–2016): Quantifying the limits of regional-scale earthquake mitigation measures. Geology 46 (3), 215–218.
Sheng, Z., Devere, J., 2005. Understanding and managing the stressed Mexico-USA transboundary Hueco Bolson Aquifer in the El Paso Del Norte Region as a complex system. Hydrgeol. J. 13, 813–825.
Arthur, J. D., Cowart, J. B., Dabous, A. A. (2001). Florida aquifer storage and recovery geochemical study: Year three progress report. Number 83. Florida Geological Survey, Tallahassee, FL, USA.
Powars, D. S. (2000). The effects of the Chesapeake Bay impact crater on the geologic framework and the correlation of hydrogeologic units of southeastern Virginia, south of the James River. Number 1622. US Geological Survey, Reston, VA.
Powars, D., Poag, C., and Mixon, R. (1993). The Chesapeake Bay "impact crater"—stratigraphic and seismic evidence. In Geological Society of America Abstracts with Programs, volume 25, pages A–378.
Poag, C.W., Powars, D.S., Poppe, L.J., Mixon, R.B., 1994. Meteoroid mayhem in ole Virginny: Source of the North American tektite strewn field. Geology 22 (8), 691–694.
Poag, C.W., 1996. Structural outer rim of Chesapeake Bay impact crater: Seismic and bore hole evidence. Meteorit. Planet. Sci. 31 (2), 218–226.
Johnson, G.H., Kruse, S.E., Vaughn, A.W., Lucey, J.K., Hobbs III, C.H., Powars, D.S., 1998. Postimpact deformation associated with the late Eocene Chesapeake Bay impact structure in southeastern Virginia. Geology 26 (6), 507–510.
Powars, D. S., Bruce, T. S., et al. (1999). The effects of the Chesapeake Bay impact crater on the geological framework and correlation of hydrogeologic units of the lower York-James Peninsula, Virginia. Technical report, United States Geological Survey. Professional Paper 1612.
Horton, J. W., Powars, D. S., & Gohn, G. S. (Eds.). (2005). Studies of the Chesapeake Bay impact structure: the USGS-NASA Langley corehole, Hampton, Virginia, and related coreholes and geophysical surveys (No. 1688). US Geological Survey.
Catchings, R. D., Powars, D. S., Gohn, G. S., & Goldman, M. R. (2002, May). High-Resolution Seismic Reflection Survey of the Southwestern Margin of the Chesapeake Bay Impact Structure, Virginia. In AGU Spring Meeting Abstracts (Vol. 2002, pp. T21A-05).
Poag, C. W., Hutchinson, D. R., Colman, S. M., & Lee, M. W. (1999). Seismic expression of the Chesapeake Bay impact crater: Structural and morphologic refinements based on new seismic data. GSA Special Papers, 149-164.
Pollyea, R.M., Fairley, J.P., Podgorney, R.K., McLing, T.L., 2014. Physical constraints on geologic CO2 sequestration in low-volume basalt formations. GSA Bull. 126 (3–4), 344–351.
Jayne, R.S., Wu, H., Pollyea, R.M., 2019. Geologic CO2 sequestration and permeability uncertainty in a highly heterogeneous reservoir. Int. J. Greenhouse Gas Control 83, 128–139.
Koehn, L., Romans, B.W., Pollyea, R.M., 2023. Assessing reservoir performance for geologic carbon sequestration in offshore saline reservoirs. Energy Adv. 2 (12), 2069–2084.
Caldwell, S. H. and McFarland, E. R. (2022). Shapefiles of hydrogeologic unit extents and top-surface altitude contours used in the revised hydrogeologic framework for the Virginia coastal plain southwest of the James River: U.S. geological survey data release.
McFarland, R. E. and Scott, B. T. (2006). The Virginia Coastal Plain Hydrogeologic Framework. Technical report, United States Geological Survey. Professional Paper 1731.
Heywood, C. E. and Pope, J. P. (2009). Simulation of Groundwater Flow in the Coastal Plain Aquifer System of Virginia. Technical report, US Geological Survey.
Masterson, J. P., Pope, J. P., Monti Jr, J., Nardi, M. R., Finkelstein, J. S., and McCoy, K. J. (2013). Hydrogeology and hydrologic conditions of the northern Atlantic coastal plain aquifer system from long Island, New York, to North Carolina. Technical report, US Geological Survey.
Clauser, C., 1992. Permeability of crystalline rocks. Eos Trans. AGU 73 (21), 233–238.
Manning, C.E., Ingebritsen, S.E., 1999. Permeability of the continental crust: Implications of geothermal data and metamorphic systems. Rev. Geophys. 37 (1), 127–150.
Saar, M.O., Manga, M., 2004. Depth dependence of permeability in the Oregon Cascades inferred from hydrogeologic, thermal, seismic, and magmatic modeling constraints. J. Geophys. Res. Solid Earth 109 (B4).
Poag, C. W. (1998). The Chesapeake Bay bolide impact: a new view of coastal plain evolution (No. 049-98). US Geological Survey.
Jung, Y., Pau, G.S.H., Finsterle, S., Pollyea, R.M., 2017. TOUGH3: A new efficient version of the TOUGH suite of multiphase flow and transport simulators. Comput. Geosci. 108, 2–7.
Deutsch, C.V., 1999. Reservoir modeling with publicly available software. Comput. Geosci. 25 (4), 355–363.
Reasenberg, P.A., Simpson, R.W., 1992. Response of regional seismicity to the static stress change produced by the Loma Prieta earthquake. Science 255, 1687–1690.
Keranen, K.M., Weingarten, M., Abers, G.A., Bekins, B.A., Ge, S., 2014. Sharp increase in central Oklahoma seismicity since 2008 induced by massive wastewater injection. Science 345 (6195), 448–451.
Poag, W., Koeberl, C., Reimold, W.U., 2012. The Chesapeake Bay crater: Geology and geophysics of a Late Eocene submarine impact structure. Springer Science & Business Media, Berlin.
Collins, G.S., Wünnemann, K., 2005. How big was the chesapeake bay impact: insight from numerical modeling. Geology 33 (12), 925–928.
Alghannam, M., Juanes, R., 2020. Understanding rate effects in injection-induced earthquakes. Nat. Commun. 11 (1), 3053.

Erskine, R., Vail, P., 1987. Passive margins: Seismic stratigraphy of the Exmouth Plateau. AAPG Special Volumes.

Steckler, M., Reynolds, D., Coakley, B., Swift, B., and Jarrard, R. (1993). Modelling passive margin sequence stratigraphy. Sequence stratigraphy and facies associations, pp. 19–41.

Richey, A.S., Thomas, B.F., Lo, M.-H., Reager, J.T., Famiglietti, J.S., Voss, K., Swenson, S., Rodell, M., 2015. Quantifying renewable groundwater stress with GRACE. Water Resour. Res. 51 (7), 5217–5238.

Quiroga, E., Bertoni, C., Van Goethem, M., Blazevic, L.A., Ruden, F., 2022. A 3D geological model of the Horn of Africa: New insights for hydrogeological simulations of deep groundwater systems. J. Hydrol.: Reg. Stud. 42, 101166.

FAO-SWALIM (2012). Hydrogeological survey and assessment of selected areas in Somaliland and Puntland; report no. w-20(fao-swalim (gcp/som/049/ec) project, Nairobi, Kenya). Technical report, Food and Agricultural Organization of the United Nations (FAO).

Purcell, P. (1979). The geology and petroleum potential of the Ogaden Basin, Ethiopia. Unpublished report, 80.

Opie, S., Taylor, R.G., Brierley, C.M., Shamsudduha, M., Cuthbert, M.O., 2020. Climate–groundwater dynamics inferred from GRACE and the role of hydraulic memory. Earth Syst. Dyn. 11 (3), 775–791.

Munier, S., Becker, M., Maisongrande, P., Cazenave, A., 2012. Using GRACE to detect groundwater storage variations: the cases of Canning Basin and Guarani Aquifer System. Int. Water Technol. J. 2, 2–13.

Government of Western Australia. (2012). West canning basin groundwater allocation limit report: Water resource allocation and planning report series report no. 52. Technical report, Department of Water.

Ebraheem, A., Riad, S., Wycisk, P., Seif El-Nasr, A., 2002. Simulation of impact of present and future groundwater extraction from the non-replenished Nubian Sandstone Aquifer in southwest Egypt. Environ. Geol. 43, 188–196.

Ebraheem, A.-A. E. (2003). A groundwater flow model for the New Valley area with a telescoping mesh on Kharga Oasis, Western Desert, Egypt. Neues Jahrbuch für Geologie und Paläontologie-Abhandlungen, pp. 153–174.

Ebraheem, A., Garamoon, H., Riad, S., Wycisk, P., Seif El Nasr, A., 2003. Numerical modeling of groundwater resource management options in the East Oweinat Area, SW Egypt. Environ. Geol. 44, 433–447.

Ebraheem, A., Riad, S., Wycisk, P., Sefelnasr, A., 2004. A localscale groundwater flow model for groundwater resources management in Dakhla Oasis, SW Egypt. Hydrgeol. J. 12, 714–722.

Voss, C.I., Soliman, S.M., 2014. The transboundary non-renewable Nubian Aquifer System of Chad, Egypt, Libya and Sudan: classical groundwater questions and parsimonious hydrogeologic analysis and modeling. Hydrgeol. J. 22 (2), 441.

Sefelnasr, A., Gossel, W., Wycisk, P., 2015. Groundwater management options in an arid environment: the Nubian Sandstone Aquifer system, Eastern Sahara. J. Arid Environ. 122, 46–58.